Organic Transistors with Ordered Nanoparticle Arrays as a Tailorable Platform for Selective, *In Situ* Detection

Mallory L. Hammock,[†] Anatoliy N. Sokolov,[†] Randall M. Stoltenberg,[‡] Benjamin D. Naab,[‡] and Zhenan Bao[†,*]

[†]Department of Chemical Engineering, and [‡]Department of Chemistry, Stanford University, Stanford, California 94305, United States

ABSTRACT

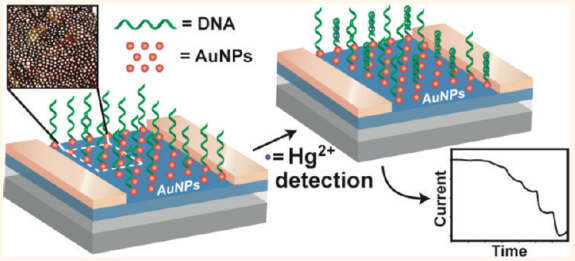

The use of organic transistors as sensing platforms provides a number of distinct advantages over conventional detection technologies, including their tunability, portability, and ability to directly transduce binding events without tedious and expensive labeling procedures. However, detection efforts using organic transistors lack a general method to uniquely specify and detect a target of interest. While highly sensitive liquid- and vapor-phase sensors have been previously reported, detection has been restricted either to the serendipitous interaction of the analyte molecules with the organic semiconductor or to the covalent functionalization of the semiconductor with receptor groups to enhance specificity. However, the former technique cannot be regularly relied upon for tailorable sensing while the latter may result in unpredictable decreases in electronic performance. Thus, a method to provide modular receptor sites on the surface of an organic transistor without damaging the device will significantly advance the field, especially regarding biological species detection. In this work, we utilized a block copolymer to template ordered, large-area arrays of gold nanoparticles, with sub-100 nm center-to-center spacing onto the surface of an organic transistor. This highly modular platform is designed for orthogonal modification with a number of available chemical and biological functional groups by taking advantage of the well-studied gold–thiol linkage. Herein, we demonstrate the functionalization of gold nanoparticles with a mercury-binding oligonucleotide sequence. Finally, we demonstrate the highly selective and robust detection of mercury(II) using this platform in an underwater environment.

KEYWORDS: organic thin-film transistors · block copolymer templating · nanoparticles · real-time detection · *in situ* sensors · mercury sensors

Organic thin-film transistors (OTFTs) provide a unique platform for chemical[1−5] and biological[3,6] detection, as well as for pressure sensors.[7−9] Such sensors offer unique tunability, portability, and the ability to directly transduce an analyte-binding event into an electrical signal, abating the need for expensive labeling and detection equipment.[10,11] The increased biocompatibility of OTFTs over their inorganic counterparts makes them attractive for biological sensing applications.[12] Additionally, the compatibility of these sensors with large-area fabrication techniques (*e.g.*, printing) makes them theoretically inexpensive to produce. OTFT-based sensors have two particularly important features; they are well suited to miniaturization and have low power requirements, making them amenable to portable sensing applications. These properties allow for their potential use as real-time diagnostic tools in the field.

Traditionally, OTFT sensors have been used for vapor-phase detection through the serendipitous sensitivity of the semiconductor material to a number of chemical moieties.[1] Identification of a particular molecule occurs through a "fingerprinting approach," in which a change in the electronic output, unique to each chemical compound tested, is matched to a previously recorded catalogue of sensor responses.[13] These sensors are extremely sensitive; the detection limit has been demonstrated down to the part-per-billion level in both the vapor and liquid phases.[11] However, this approach suffers from a lack of true selectivity, as it relies upon the semiconductor's inherent sensitivity to many chemical species. Though some efforts have been made to tune the sensor's selectivity by chemically altering the semiconductor[11,14,15] or through the addition of sensory layers,[16,17] the ability to uniquely detect a predetermined analyte is a challenge that will require the incorporation of more specific recognition sites.

Many OTFT sensors are restricted to detection in the vapor phase as a result of their high operation voltage and instability under aqueous conditions; however, operation in liquids is equally important for sensing.[12,18] As a response to the growing number of sensor applications requiring detection of

* Address correspondence to zbao@stanford.edu.

Received for review December 9, 2011 and accepted March 7, 2012.

Published online March 07, 2012
10.1021/nn204830b

aqueous-phase analytes, our group developed water-stable OTFT sensors[6] and carbon nanotube transistor sensors[19] capable of detecting a number of small molecules in solution. These sensors were capable of low-voltage operation due to the incorporation of an ultrathin dielectric layer and a water-stable semiconductor. However, while the active layer was inherently sensitive to several species, the ability to specify an affinity for a particular molecule has, thus far, been limited. The use of a traditional fingerprinting approach to identify the constituents of complex aqueous mixtures (*e.g.*, the detection of biological molecules in media or environmental contaminants in natural water sources) would require the development of a number of organic semiconductors capable of stable operation within the media in order to catalogue the responses to the vast number of species present in these samples.

A more practical method of enabling selective sensing in these complex mixtures is the incorporation of specific recognition sites into a single, stable, organic semiconductor layer. However, the covalent modification of the organic semiconductor can lead to unpredictable decreases in device performance, changes in thin-film morphology, and loss of stability.[11,15,20] Moreover, the gram-scale attachment of biological molecules directly to the semiconductor backbone may be an expensive endeavor. Therefore, a method to introduce attachment sites on the surface of an OTFT without covalently modifying the semiconductor would provide a significant advantage for the detection of biological species in aqueous environments.

Recently, the attachment of capture sites for biomolecules was accomplished *via* the introduction of an insulating polymer with covalent attachment sites on top of the active semiconductor.[21,22] However, this approach results in a polymer film between the analyte and the active semiconductor layer, thus preventing their direct interaction. We sought to integrate binding sites in a manner that allows for more direct interaction between the semiconductor and analyte by depositing an array of regularly spaced nanoparticles (NPs) onto the sensor surface. Previously, disordered arrays of NPs have been incorporated in ion-sensitive field effect transistors (ISFETs) through layer-by-layer incorporation into the active layer,[23,24] in chemiresistors and in inorganic transistors through the chemical modification of the silicon surface to attract NPs,[4,23,25] as well as in transistors comprised of nanotube networks[26] and graphene.[27] However, the incorporation of highly ordered NP arrays onto the surface of an OTFT, theoretically allowing for more reproducible and controllable sensing experiments, has not yet been demonstrated.

An ordered array of individual particles on the surface is needed for the realization of optimized detection with NPs, as it will allow for a higher density[28] and more uniform distribution of attachment sites, resulting in more reproducible sensors. However, the nanoscale patterning of NPs is difficult to achieve without resorting to expensive or tedious patterning techniques (*e.g.*, lithography, microcontact printing, or direct surface patterning).[23,29] Block copolymers have been praised for their ability to form nanoscale features through self-assembly and offer sub-10 nm patterning with simple processing procedures (*e.g.*, spin coating).[30] For example, poly(styrene-*b*-4-vinylpryidine) (PS-*b*-P4VP) is known to form a hexagonally close-packed array of core−shell micelles.[30] The pyridine core of the micelle can be loaded with metal or metal oxide precursors, that, following the removal of the polymer, result in large-area, highly ordered patterns of NPs.[31] The arrays are highly adaptable, as the precursors can be varied to change the composition of the NPs. Herein, we use this technique to deposit gold NPs (AuNPs) in order to provide modular attachment points on the surface of an OTFT. Because the AuNPs can be selectively modified through thiol-based chemistry to avoid the direct modification of the OTFT surface, our system provides a means of device sensitization that is orthogonal to the surface chemistry of the organic semiconductor. This modularity allows for a wider range of analytes and semiconductors to be implemented in the sensor platform than would be possible if the sensing mechanism depended directly on inherent analyte-semiconductor interactions. Additionally, the spacing between NPs can be tailored by varying the molecular weight of the block copolymer, adding yet another dimension of flexibility to this system. For the application in this work, the AuNP spacing is not thought to be crucial; however, for future biosensing applications, the ability to tune the distance between the attachment sites may be important. For these cases, engineering the NP center-to-center spacing to match the analyte's molecular footprint will allow for a higher density of NPs to be incorporated onto the surface while still preventing potential aggregation and steric hindrance of the captured analytes.

As a proof-of-concept demonstration of this platform's selective sensing capability, a DNA-based probe for mercury (Hg^{2+}) was attached to the AuNPs, resulting in a highly selective Hg^{2+} sensor. As Hg^{2+} is a highly toxic and widespread contaminant, whose accumulation in the environment is extremely hazardous, the Environmental Protection Agency regulates its concentration in drinking water to levels on the order of 1 nM.[32,33] While there exist a number of state-of-the-art sensors that can detect Hg^{2+} to this level[34] based on fluorometric, colorimetric, and electrochemical techniques, these systems are heavily dependent upon bulky supporting electronic equipment. This dependence prevents their use in the field, where real-time information is critical. Thus, low-power, highly portable sensors, such as those afforded by

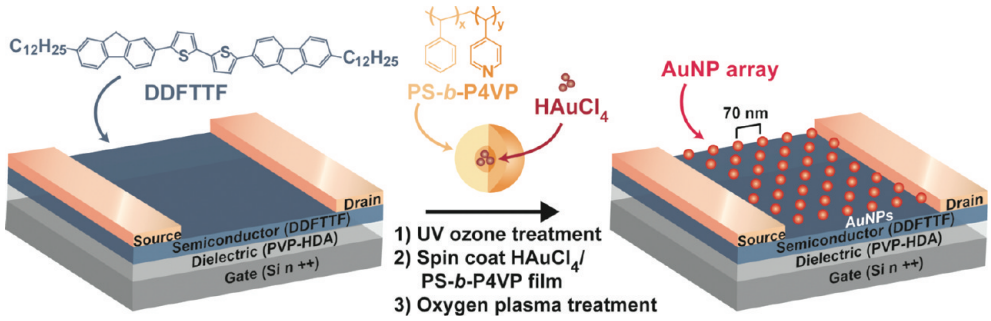

Figure 1. Fabrication of the sensor platform. A water-stable transistor with an ultrathin PVP-HDA dielectric and DDFTTF semiconductor is treated with UV ozone to activate the surface. AuNP precursors are introduced by spin coating a polymeric matrix (PS-*b*-P4VP) containing $HAuCl_4$. The device is exposed to oxygen plasma to remove the PS-*b*-P4VP and convert $HAuCl_4$ to Au^0, thus forming an ordered array of AuNPs, with 70 nm center-to-center spacing.

OTFTs, may soon become critical components of environmental regulation in the field.

RESULTS AND DISCUSSION

Building upon our previous work,[6] we utilized a water-stable transistor architecture containing an ultrathin layer of poly(4-vinylphenol) (PVP) cross-linked with 4,4′-(hexafluoroisopropylidene)dipthalic anhydride (HDA) as the dielectric and the small molecule 5,5′-bis-(7-dodecyl-9*H*-fluoren-2-yl)-2,2′-bithiophene (DDFTTF) as the semiconductor (Figure 1, left). These materials were selected to facilitate underwater operation, which is critical for enabling real-time sensing applications *in situ*. In its current form, however, this platform lacks the inherent ability to sense specifically defined targets, and the traditional methods of directly modifying the semiconductor to affix binding sites (*e.g.*, introduction of receptors either through chemical modification or physical immobilization) can degrade transistor performance.[11,20] Thus, to increase the modularity of these OTFT sensors for the selective detection of a wide range of possible analytes, we nanopatterned the surface of the transistor with an ordered array of AuNPs (Figure 1, right).

By incorporating a gold salt, hydrogen tetrachloroaurate ($HAuCl_4$), within the pyridine block in the PS-*b*-P4VP micelles, large-area, ordered arrays of AuNP precursors were deposited onto a UV ozone-activated OTFT *via* a simple spin coating method.[31] Removal of the PS-*b*-P4VP and conversion of the $HAuCl_4$ to metallic Au^0 with oxygen plasma resulted in the formation of highly reproducible, large-area arrays of AuNPs with 70 nm center-to-center spacing. AuNPs were specifically chosen for this application as their widespread use has generated a rich library of available thiolated capture probes to target nearly any analyte of interest.[35,36] By combining a water-stable transistor with block copolymer-templated AuNP arrays, we have developed a highly tailorable platform that affords facile compatibility with a wide range of target molecules for selective sensing applications.

Charge carrier mobility (μ) is highly affected by the morphology of the active layer in the channel; therefore, obtaining two-dimensional growth of the semiconductor is critical in optimizing OTFT performance.[37−39] We have also found that planar morphology plays a critical role in determining the AuNP distribution on the surface. The previously reported deposition conditions for DDFTTF[6] lead to suboptimal NP dispersion on the sensor surface, as they produced highly disordered, nonplanar surfaces (Supporting Information, Figures S1A and S2). In this work, it was determined the temperature of the substrate (T_{sub}) during evaporation played the predominant role in determining semiconductor morphology. High T_{sub} likely enhances surface diffusion of the evaporated DDFTTF molecules as they deposit onto the surface, allowing for the formation of smooth, two-dimensional surfaces.[38] The optimized conditions utilized a PVP-HDA substrate maintained at 195 °C during the thermal evaporation of 30 nm of DDFTTF, resulting in highly planar surfaces over large areas (Figure 2A,B; see Supporting Information text and Figures S1, S3, and S4 for full range of optimization conditions). These planar surfaces facilitate the spin coating process, giving rise to ordered arrays of AuNPs (Figure 2C). Despite the variation in AuNP size and shape, the AuNPs are readily functionalizable, resulting in viable analyte-binding sites. As a control experiment to verify that the devices could not be more easily functionalized with AuNPs from a colloidal solution, a commercially purchased solution of 5 nm AuNPs was drop cast onto devices. The concentration of the commercially purchased solution of AuNPs was approximately 80 nM, while the concentration of the micelles containing the AuNP precursors was approximately 70 nM. Visual inspection of the surface revealed that the colloidal AuNP treatment led to the formation of nonuniform aggregates (Figure 2D), and rinsing the devices in deionized water to remove these aggregates resulted in cracking and delamination of the electrodes, as well as removal of the semiconductor and dielectric

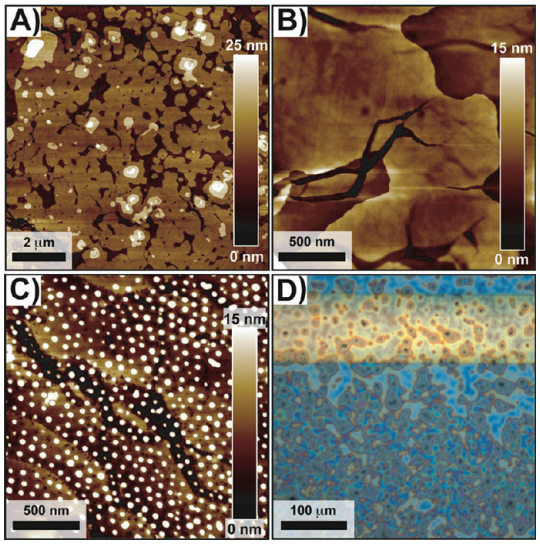

Figure 2. Sensor morphology during various stages of device fabrication as measured with AFM operated in the tapping mode. (A) Height image of large-area, planar morphology of DDFTTF, achieved using elevated T_{sub} (195 °C) during thermal evaporation. Zoomed in height images of surface morphology (B) before and (C) after AuNP deposition. (D) Optical micrograph of device with colloidal AuNPs drop cast onto device surface. An AFM image of the device containing randomly spaced colloidal AuNPs was not available due to the extremely rough nature of this surface. The corresponding μ for each stage of device fabrication is found in Supporting Information, Table 1S.

layers, rendering the devices incapable of undergoing electronic testing (Supporting Information, Figure S5).

The orthogonal gold–thiol (Au–S) chemistry afforded by the AuNPs allows for their modification independent of the semiconductor. The pre-existing abundance of thiolated chemicals allows for the incorporation of a broad range of molecules onto the surface of the sensor.[35,36] To take advantage of this chemistry, we exposed the devices to a thiolated DNA oligomer that binds Hg^{2+} by virtue of a series of thymine–thymine mismatches (Figure 3A).[40,41] Previously, DNA has been immobilized onto OTFT surfaces;[42] however, as we demonstrate, exposure to ionic solutions (*e.g.*, buffers) may remove nonspecifically bound DNA, leading to poor reproducibility. Thus, covalently binding the DNA to the AuNPs will provide for a controlled, robust functionalization and lead to increased sensor reproducibility.

X-ray photoelectron spectroscopy (XPS) of phosphorus (Figure 3B) and nitrogen (Figure 3C) groups on the sensor surface verified the successful functionalization of the AuNPs with DNA (DNA–AuNPs). Before DNA functionalization, there was no phosphorus on the surface (pink trace, Figure 3B). The marked growth of the phosphorus (P 2p) signal after chemical modification (black trace, Figure 3B) clearly demonstrates the presence of DNA on the surface. There were two sources of nitrogen within the device. First, residual nitrogen that originated from the deposition of the AuNPs in a PS-*b*-P4VP matrix was present prior to introducing the DNA (pink trace, Figure 3C). Second, the DNA itself contained nitrogen groups. The contribution to the nitrogen signal from the oligonucleotide is identifiable by a +1 eV shift in the nitrogen (N 1s) binding energy (black trace, Figure 3C), resulting from the more electropositive chemical environment of some of the nitrogens found in DNA compared to the pyridine-containing polymer.[43,44] The heights of the AuNPs were also measured with atomic force microscopy (AFM) in the dry state before and after functionalization with DNA (Supporting Information, Figure S6). The average height of the AuNPs was found to increase by 1.6 nm after the DNA modification, providing additional evidence of the successful reaction.

Biological molecules are known to exhibit nonspecific binding to some surfaces. This "biofouling" commonly degrades device specificity and performance.[45] Thus, a salt rinse was employed to remove noncovalently bound oligonucleotides (Supporting Information, Figure S7).[46] To demonstrate that post-rinsing, the oligonucleotide was specifically bound to the AuNPs and not to the semiconductor surface, a device was fabricated without AuNPs ($HAuCl_4$ was not added to the PS-*b*-P4VP matrix, red trace, Figure 3B,C) and exposed to DNA (DNA–PS-*b*-P4VP). The lack of a phosphorus signal and absence of a shift in the nitrogen trace indicate that nonspecifically bound oligonucleotides are not present after the salt rinse. Thus, the Au–S chemistry provides a method to covalently incorporate selective binding sites for an arbitrary analyte of interest (*e.g.*, Hg^{2+}) exclusively onto the AuNPs, leaving the semiconductor unmodified.

To ensure device stability throughout the fabrication process, output (drain–source voltage (V_{DS}) = 0.0 → −0.6 V, gate-source voltage (V_{GS}) = 0.25 → −1.0 V) and transfer plots (V_{DS} = −0.6 V, V_{GS} = 0.60 → −1.0 V) were obtained under ambient and aqueous conditions (Supporting Information, Table S1 and Figure S8). The applied V_{DS} was limited to a magnitude of 0.6 V in order to prevent ionic conduction through the water droplet that was placed on top of the device for operation under aqueous conditions. Despite exposure to both UV ozone and oxygen plasma, the sensors remained functional p-type transistors (Figure 4A, Supporting Information, Figures S9 and S10), with μ as high as 0.25 $cm^2\ V^{-1}\ s^{-1}$ (μ_{avg} of 0.18 $cm^2\ V^{-1}\ s^{-1}$), an on/off ratio of 2×10^3, and a threshold voltage (V_T) of 0.1 V. As these values are similar to those before AuNP deposition (Supporting Information, Table S1) as well as those previously reported,[6] the incorporation of AuNPs onto the OTFT's surface does not significantly diminish device performance. Additionally, the sensor platform was found to remain stable under aqueous operating conditions (Figure 4B), with μ as high as

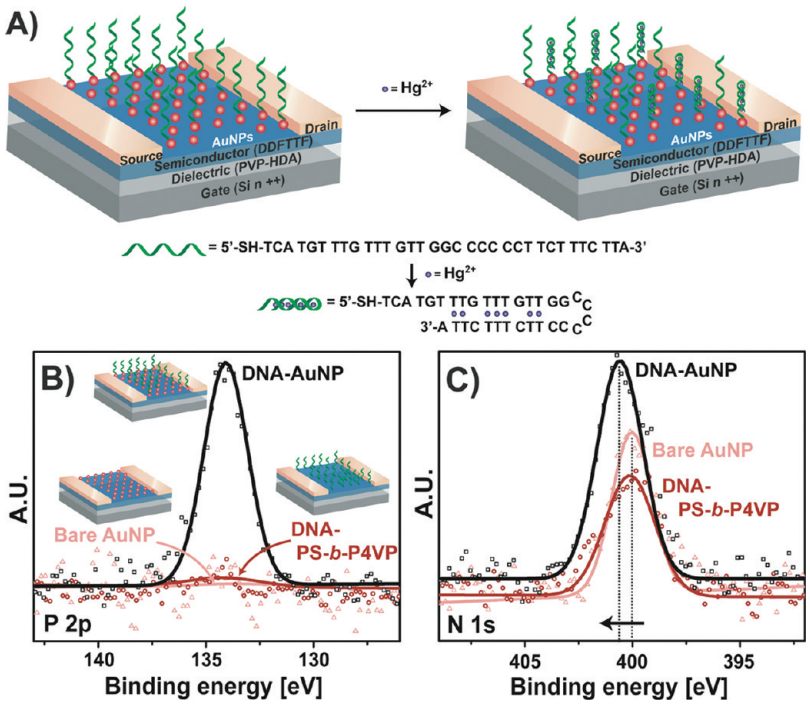

Figure 3. Independent functionalization of AuNPs with an Hg^{2+}-binding DNA sequence. (A) Schematic representation of the functionalization of AuNPs with a thiolated Hg^{2+}-binding oligonucleotide[40] and subsequent Hg^{2+} capture by the DNA. XPS of the (B) phosphorus (P 2p) and (C) nitrogen (N 1s) regions before (pink trace) and after (black trace) DNA exposure, showing development of the P 2p peak and augmentation and +1 eV shift of the N 1s peak. Thiolated DNA was also added to a device without AuNPs (red trace) to demonstrate that only covalently bound DNA was present.

0.16 $cm^2\ V^{-1}\ s^{-1}$ (μ_{avg} of 0.09 $cm^2\ V^{-1}\ \ s^{-1}$), an on/off ratio of 5×10^1, and a V_T of 0.8 V. It should be noted that the μ reported here for underwater operation was not corrected for the incorporation of water within the PVP-HDA dielectric during prolonged exposure to water (unpublished data). The sensor's ability to function underwater dramatically increases its impact for the multitude of sensing applications that require real-time measurements *in situ* (*e.g.*, protein, DNA, or metal ion detection).

Upon introduction of Hg^{2+} to the DNA−AuNP sensor, the Hg^{2+}-binding aptamer undergoes a conformational change[40] (Figure 3A and Supporting Information, Figure S11) to form a hairpin structure, which increases the negative charge density at the surface. This increased negative charge density subsequently induces positive charges in the semiconductor according to the field effect,[42,47−49] which ultimately results in an increase of the drain−source current (I_{DS}) in the p-type transistor. During the cumulative addition of Hg^{2+} to the sensor, detection of Hg^{2+} concentrations on the order of 1 μM (Figure 4C) were possible. Slight variation in the absolute value of the sensor response between devices arose from batch-to-batch variability during the fabrication process as well as the limitations associated with using a sessile droplet rather than a flow cell for aqueous sensing measurements. While state-of-the-art systems may reach lower detection limits,[50,51] rapid readout (on the order of minutes), ease of synthesis, and portability distinguish this platform for applications in the field. Though it was beyond the scope of this work, lower detection limits could potentially be achieved by increasing the AuNP density to increase the concentration of Hg^{2+}-binding oligonucleotides present on the surface.

The sensing mechanism was investigated by regenerating the sensor with a five-minute rinse in deionized water in order to remove Hg^{2+} bound by the DNA. Regeneration of the device through traditional methods of DNA denaturation (temperature or pH variation) was not possible owing to the pre-existing sensitivity of the semiconductor to these variables.[6] The difference of rinsing with deionized water *versus* the previously described salt solution was negligible. Initial exposure of the DNA−AuNP sensor to Hg^{2+} resulted in a large increase in the magnitude of the I_{DS} (Figure 5A, black trace), whereas devices with bare AuNPs (Figure 5A, dark red trace), devices without AuNPs (Figure 5A, red trace), and devices with unmodified DDFTTF (Figure 5A, pink trace) showed only a weak response to very high concentrations of Hg^{2+}. Since the magnitude of the response for the DNA-functionalized devices was consistently larger than those lacking DNA, the device's sensitivity for Hg^{2+} can be primarily attributed to the incorporation of the Hg^{2+}-binding DNA

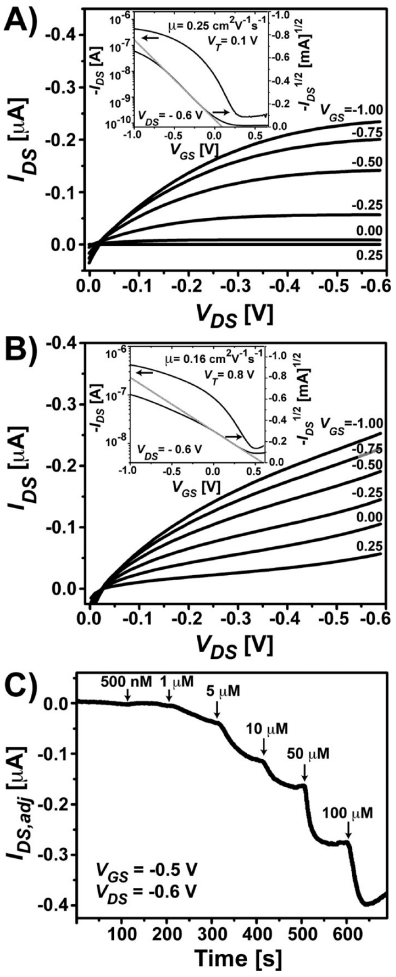

Figure 4. Electrical characterization of the DNA−AuNP sensor platform. Output (V_{GS} = 0.25 → −1.0 V) and transfer (V_{DS} = −0.6 V, inset) plots of the sensor (A) before and (B) after exposure to water. (C) I_{DS} versus time response of the platform to increasing concentrations of Hg^{2+} (V_{GS} = −0.5 V, V_{DS} = −0.6 V), where the baseline current has been subtracted ($I_{DS,adj}$). Arrows in panel C designate the addition of Hg^{2+} at the indicated concentration. The device was sensitive to Hg^{2+} concentrations on the order of 1 μM.

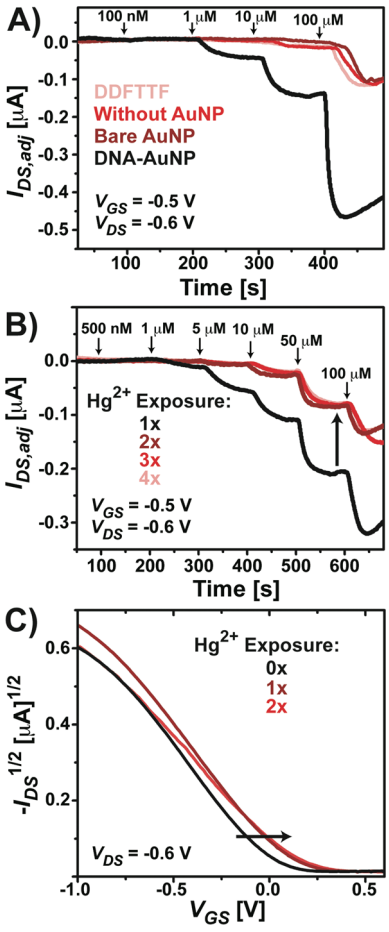

Figure 5. Regeneration of the sensor platform. (A) $I_{DS,adj}$ *versus* time response of the sensor during various stages of fabrication, indicating a slight sensitivity to Hg^{2+} prior to DNA functionalization of the AuNPs (V_{GS} = −0.5 V, V_{DS} = −0.6 V). (B) $I_{DS,adj}$ *versus* time response of a single device during primary (black trace), secondary (dark red trace), tertiary (red trace), and quaternary (pink trace) exposures to Hg^{2+} (V_{GS} = −0.5 V, V_{DS} = −0.6 V). Arrows in panels A and B designate the addition of Hg^{2+} at the indicated concentration. (C) Square root plot (V_{DS} = −0.6 V) of the same dry device prior to (black trace) and after (dark red and red traces) multiple exposures to Hg^{2+}.

sequence. The weak response of the devices lacking DNA to Hg^{2+} may result from doping of the semiconductor itself, as has been previously observed for the detection of Hg^{2+} with carbon nanotubes,[32] or through charge transfer between Hg^{2+}, Au^0 (either the AuNP or the unpassivated sides of the electrodes), and the semiconductor.[52,53] Subsequent exposure of the devices lacking DNA to Hg^{2+} resulted in minimal signal (Supporting Information, Figure S13), suggesting that any interaction between the semiconductor and Hg^{2+} is irreversible. To test for the reversibility and reproducibility of the DNA-AuNP sensor response, the device was re-exposed to Hg^{2+}. The magnitude of the response observed upon this secondary exposure was lower than that observed for the primary exposure (Figure 5B, black *versus* dark red trace), potentially due to the incomplete removal of the Hg^{2+} bound to the DNA. However, all subsequent exposures to Hg^{2+} resulted in remarkably reproducible responses (Figure 5B, dark red, red, and pink traces) and a positive shift in V_T (from 0.02 to 0.11 V, Figure 5C) was observed after Hg^{2+} exposure. Therefore, the primary sensing mechanism (Hg^{2+} binding by the DNA aptamer) is reversible, resulting in highly reproducible sensor responses.

To develop a reproducible sensor capable of Hg^{2+} detection in the field, the response to other potential contaminants must be minimized. To establish the sensor's specificity for Hg^{2+}, it was interrogated with a variety of other common environmental contaminants, including Na^+, Mg^{2+}, K^+, Ca^{2+}, Co^{2+}, Ni^{2+}, Cu^{2+}, Zn^{2+}, Pb^{2+}, and Cd^{2+} (Figure 6A). The Hg^{2+}-binding DNA sequence was previously found to be highly selective for Hg^{2+} when tested against a

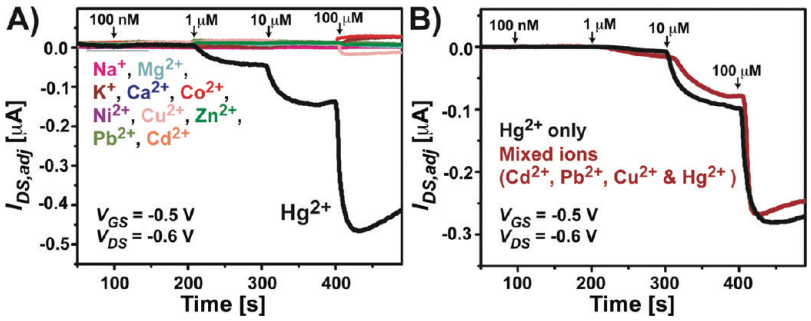

Figure 6. Selectivity and interference testing of the sensor platform. (A) $I_{DS,adj}$ *versus* time response of the sensor upon interrogation with a variety of individual metal ions ($V_{GS} = -0.5$ V, $V_{DS} = -0.6$ V). (B) $I_{DS,adj}$ *versus* time response of the sensor upon interrogation with a mixture of metal ions (Cd^{2+}, Pb^{2+}, Cu^{2+}, and Hg^{2+}, each at the indicated concentration, $V_{GS} = -0.5$ V, $V_{DS} = -0.6$ V). Arrows in panels A and B designate the addition of Hg^{2+} at the indicated concentration.

subset of these ions.[40] The addition of many of these ions resulted in a slight decrease in the magnitude of I_{DS}. This response may have resulted from the increased ionic conductivity within the water droplet, prompting current flow through the water rather than through the channel. Additionally, both DNA-functionalized and nonfunctionalized devices demonstrated a slight affinity for Cu^{2+}, which was attributed to the interaction of Cu^{2+} with a small quantity of oxidized surface states unintentionally formed during device fabrication.[54,55] These surface states may have resulted from the oxidation of residual PS-*b*-P4VP[54] to carboxylic acid species. However, we discovered that this interaction is largely irreversible, and that pre-exposing the device to a dilute solution of all of the ions except Hg^{2+} during the fabrication process quenched the Cu^{2+} sensitivity. Finally, the sensor's ability to detect Hg^{2+} in complex solutions was investigated. When interrogated with a complex sample containing multiple ionic species (Cd^{2+}, Pb^{2+}, Cu^{2+}, and Hg^{2+}), the sensor was able to detect Hg^{2+} without interference (Figure 6B). Ultimately, the high selectivity of the sensing platform for Hg^{2+} demonstrates the ability to engineer specificity for a chosen target, while the platform's ability to operate without interference in complex solutions demonstrates its viability for specific detection in highly complex media.

CONCLUSIONS

By combining a water-stable OTFT with block copolymer-templated AuNPs, we developed a modular sensing platform exhibiting specific recognition sites that are available for modification through orthogonal surface chemistry techniques. We subsequently functionalized the AuNPs to produce a specific binding site for an analyte of our choosing (in this application, Hg^{2+}). We demonstrated the sensor's ability to selectively detect our chosen target *in situ*, as well as its ability to produce a clear detection profile when operating in a solution of interferant ions. This platform is highly versatile due to the immense library of chemicals available for AuNP functionalization as well as tunable AuNP spacing. Moreover, the use of metal−oxide nanoparticles can, in the future, expand the library of orthogonal chemistry beyond the Au−S linkage. Though a full study is beyond the scope of this work, it is anticipated that the spacing of the AuNPs is particularly important for sensing applications involving biomolecules,[56] where aqueous real-time sensing *in situ* is needed.

METHODS

DDFTTF Synthesis. The organic semiconductor, DDFTTF, was synthesized according to literature procedures,[57] except that a microwave reactor (CEM Discover-S) was used in the final coupling step. Briefly, 2-bromo-9-dodecyl-fluorene (4.912 mmol), bis-2−2′-(trimethylstannyl)bithiophene (2.34 mol), $Pd(PPh_3)_4$ (4 mol %), and 20 mL of argon-purged toluene were mixed in a microwave tube. The mixture was exposed to microwave radiation with stirring (high power of 300 W) for 25 min while the temperature was varied between 125 and 165 °C. Upon completion of the reaction, the solution was vacuum filtered, and the solid fraction was rinsed with 50−75 mL of toluene and 150 mL of methanol to give crude DDFTTF (1.65 g, 85% yield). Prior to use, the crude product was purified three times by gradient vacuum sublimation at 1×10^{-5} Torr.

Device Fabrication and AuNP Incorporation. A cross-linked polymer dielectric (PVP-HDA) was formed according to literature procedures[58] and a film was deposited onto highly doped (n ++), ⟨100⟩ orientation, native oxide Si wafers (Silicon Quest International) by spin coating (Headway Research) at 4000 rpm. A 30 nm DDFTTF film was deposited using thermal evaporation (Angstrom Engineering) utilizing an evaporation rate of 0.2 A s^{-1} and a T_{sub} of 195 °C to ensure two-dimensional device morphology. Metal salt-containing PS-*b*-P4VP (M_n PS = 55 kDa, M_n P4VP = 50 kDa) solutions were prepared according to literature conditions,[31] except that $HAuCl_4$ (Premion) was substituted for $AlCl_3$. Films of $HAuCl_4$-containing polymeric micelles were deposited by spin coating the solutions at 5000 rpm for 40 s onto a device that had previously been activated with UV ozone (Jetlight) for 4.0 min. Activation of the device with UV ozone ensured the formation of a continuous film of the

copolymer on the semiconductor surface. Previously this activation with UV ozone was utilized to achieve the deposition of polymer electrodes on the surface of the semiconductor without the degradation of device performance.[59] The polymer matrix was subsequently removed by exposing the device to oxygen plasma (GaLa Instrumente) for 0.4 min (0.4 mbar of O_2, 80 W). Careful monitoring of the exposure time to both UV ozone and oxygen plasma was critical, as overexposure of the organic semiconductor to these harsh conditions destroyed transistor performance. Transistors were fabricated in the top-contact geometry, with source and drain electrodes (Au) evaporated through a shadow mask on a rotating substrate at a rate of 2 A s^{-1}. Electrode dimensions were defined to have a channel width of 4 mm and length of 50 μm. A protective layer of SiO_x was thermally evaporated exclusively over the electrodes at a rate of 0.4 A s^{-1} to minimize potential electrochemical reactions, as well as DNA binding that could occur at the electrodes.

AuNP Functionalization. Devices with AuNP arrays were re-exposed to oxygen plasma for 0.1 min to clean the AuNP surfaces. A 33-base pair thiolated oligonucleotide previously reported to bind Hg^{2+} (5′-SH-TCA TGT TTG TTT GTT GGC CCC CCT TCT TTC TTA-3′)[40] was custom synthesized by Integrated DNA Technologies. A 15 μL aliquot of a 100 μM DNA solution in 1× PBS was spotted onto the devices on top of the area protected by SiO_x, and the devices were incubated at room temperature for 90 min in a desiccator under slight vacuum. Following DNA incubation, the devices were briefly rinsed with deionized water and incubated in a salt solution (10 mM Tris-HCl, 0.5 mM ETDA, 1 M NaCl, pH 7.5) for 15 min. Subsequently the devices were exposed to a dilute (250 nM) solution of each of the metal ions tested, excluding Hg^{2+}. Finally, devices were rinsed with deionized water, re-equilibrated through a 30-min incubation in deionized water, and placed under vacuum to dry.

Device Characterization. The device morphology was characterized using a MultiMode AFM (Veeco) operated in the tapping mode. XPS (PHI 5000 Versaprobe, Al Kα source) was used to measure the elemental composition of the device surface. High-resolution spectra were collected at an angle of 45°, a pass energy of 117.4 eV, and a step size of 0.1 eV. All XPS spectra were referenced to a C 1s binding energy of 284.8 eV. OTFTs used for the XPS study were formed by spin coating an additional film of $HAuCl_4$-containing PS-*b*-P4VP onto a previously formed AuNP array to increase the AuNP density.[31] These were again exposed to oxygen plasma, and then incubated in the DNA solution as described above. Electrical measurements were carried out under ambient conditions using a two-sourcemeter (Keithley 2635 (Drain/Source) and Keithley 2400 (Gate)). For electrical testing under aqueous conditions, a 9 μL droplet of deionized water was placed on top of the device, and the device was allowed to equilibrate prior to testing. A low operating voltage ($V_{DS} = -0.6$ V, $V_{GS} = -0.5$ V) was used in order to prevent ionic conduction through the water droplet. For Hg^{2+} testing, a 1 μL droplet of 10× concentrated Hg^{2+} solution was slowly added to a 9 μL droplet of deionized water in order to dilute the Hg^{2+} to the nominal concentration indicated. To conserve the volume of the liquid droplet, a 1 μL droplet was removed after the signal had fully developed (~85 s), in order to prepare the system for the subsequent addition of concentrated Hg^{2+}.

Conflict of Interest: The authors declare no competing financial interest.

Acknowledgment. The authors thank Dr. Jeffery Tok, O. B. Johnson, O. Knopfmacher, and G. Giri for many helpful discussions. M.L.H. acknowledges funding from the National Defense Science and Engineering Graduate (NDSEG) Fellowship (32 CFR 168a) and the National Science Foundation Graduate Research Fellowship. A.N.S. would like to acknowledge financial support from the NSF-ECCS-EXP-SA program (NSF ECCS-0730710) and Office of Naval Research (N000140810654). R.M.S. acknowledges funding from the National Science Foundation Graduate Research Fellowship Program. This work also received funding from a Grand Challenges Explorations Grant (OPP1032970).

Supporting Information Available: Device optimization (including deposition conditions for the organic semiconductor and exposure times for the UV ozone and oxygen plasma treatments), the use of a salt wash to eliminate extraneous DNA, device characterization throughout fabrication, and detection mechanism. This material is available free of charge *via* the Internet at http://pubs.acs.org.

REFERENCES AND NOTES

1. Torsi, L.; Dodabalapur, A. Organic Thin-Film Transistors as Plastic Analytical Sensors. *Anal. Chem.* **2005**, *77*, 380A–387A.
2. Torsi, L.; Dodabalapur, A.; Sabbatini, L.; Zambonin, P. G. Multi-parameter Gas Sensors Based on Organic Thin-Film-Transistors. *Sens. Actuators, B* **2000**, *67*, 312–316.
3. Mabeck, J. T.; Malliaras, G. G. Chemical and Biological Sensors Based on Organic Thin-Film Transistors. *Anal. Bioanal. Chem.* **2006**, *384*, 343–353.
4. Tisch, U.; Haick, H. Nanomaterials for Cross-Reactive Sensor Arrays. *MRS Bull.* **2010**, *35*, 797–803.
5. Bora, M.; Schut, D.; Baldo, M. A. Combinatorial Detection of Volatile Organic Compounds Using Metal-−Phthalocyanine Field Effect Transistors. *Anal. Chem.* **2007**, *79*, 3298–3303.
6. Roberts, M. E.; Mannsfeld, S. C. B.; Queralto, N.; Reese, C.; Locklin, J.; Knoll, W.; Bao, Z. Water-Stable Organic Transistors and Their Application in Chemical and Biological Sensors. *Proc. Natl. Acad. Sci. U.S.A.* **2008**, *105*, 12134–12139.
7. Someya, T.; Sekitani, T.; Iba, S.; Kato, Y.; Kawaguchi, H.; Sakurai, T. A Large-Area, Flexible Pressure Sensor Matrix with Organic Field-Effect Transistors for Artificial Skin Applications. *Proc. Natl. Acad. Sci. U.S.A.* **2004**, *101*, 9966–9970.
8. Mannsfeld, S. C. B.; Tee, B. C. K.; Stoltenberg, R. M.; Chen, C. V. H. H.; Barman, S.; Muir, B. V. O.; Sokolov, A. N.; Reese, C.; Bao, Z. Highly Sensitive Flexible Pressure Sensors with Microstructured Rubber Dielectric Layers. *Nat. Mater.* **2010**, *9*, 859–864.
9. Lipomi, D. L.; Vosgueritchian, M.; Tee, B. C. K.; Hellstrom, S. L.; Lee, J. A.; Fox, C. H.; Bao, Z. Skin-Like Pressure and Strain Sensors Based on Transparent Elastic Films of Carbon Nanotubes. *Nat. Nanotechnol.* **2011**, *6*, 788–792.
10. Wang, L.; Fine, D.; Sharma, D.; Torsi, L.; Dodabalapur, A. Nanoscale Organic and Polymeric Field-Effect Transistors as Chemical Sensors. *Anal. Bioanal. Chem.* **2006**, *384*, 310–321.
11. Roberts, M. E.; Sokolov, A. N.; Bao, Z. Material and Device Considerations for Organic Thin-Film Transistor Sensors. *J. Mater. Chem.* **2009**, *19*, 3351–3363.
12. Berggren, M.; Richter-Dahlfors, A. Organic Bioelectronics. *Adv. Mater.* **2007**, *19*, 3201–3213.
13. Crone, B.; Dodabalapur, A.; Gelperin, A.; Torsi, L.; Katz, H. E.; Lovinger, A. J.; Bao, Z. Electronic Sensing of Vapors with Organic Transistors. *Appl. Phys. Lett.* **2001**, *78*, 2229–2231.
14. Torsi, L.; Tanese, M. C.; Cioffi, N.; Gallazzi, M. C.; Sabbatini, L.; Zambonin, P. G. Alkoxy-Substituted Polyterthiophene Thin-Film-Transistors as Alcohol Sensors. *Sens. Actuators, B* **2004**, *98*, 204–207.
15. Huang, J.; Miragliotta, J.; Becknell, A.; Katz, H. E. Hydroxy-Terminated Organic Semiconductor-Based Field-Effect Transistors for Phosphonate Vapor Detection. *J. Am. Chem. Soc.* **2007**, *129*, 9366–9376.
16. Torsi, L.; Farinola, G. M.; Marinelli, F.; Tanese, M. C.; Omar, O. H.; Valli, L.; Babudri, F.; Palmisano, F.; Zambonin, P. G.; Naso, F. A Sensitivity-Enhanced Field-Effect Chiral Sensor. *Nat. Mater.* **2008**, *7*, 412–417.
17. Sokolov, A. N.; Roberts, M. E.; Johnson, O. B.; Cao, Y.; Bao, Z. Induced Sensitivity and Selectivity in Thin-Film Transistor Sensors *via* Calixarene Layers. *Adv. Mater.* **2010**, *22*, 2349–2353.
18. Someya, T.; Dodabalapur, A.; Gelperin, A.; Katz, H. E.; Bao, Z. Integration and Response of Organic Electronics with Aqueous Microfluidics. *Langmuir* **2002**, *18*, 5299–5302.

19. Roberts, M. E.; LeMieux, M. C.; Bao, Z. Sorted and Aligned Single-Walled Carbon Nanotube Networks for Transistor-Based Aqueous Chemical Sensors. *ACS Nano* **2009**, *3*, 3287–3293.
20. Sokolov, A. N.; Roberts, M. E.; Bao, Z. A. Fabrication of Low-Cost Electronic Biosensors. *Mater. Today* **2009**, *12*, 12–20.
21. Khan, H. U.; Roberts, M. E.; Johnson, O. B.; Förch, R.; Knoll, W.; Bao, Z. *In Situ*, Label-Free DNA Detection Using Organic Transistor Sensors. *Adv. Mater.* **2010**, *22*, 4452–4456.
22. Khan, H. U.; Jang, J.; Kim, J.-J.; Knoll, W. *In Situ* Antibody Detection and Charge Discrimination Using Aqueous Stable Pentacene Transistor Biosensors. *J. Am. Chem. Soc.* **2011**, *133*, 2170–2176.
23. Ibañez, F. J.; Zamborini, F. P. Chemiresistive Sensing with Chemically Modified Metal and Alloy Nanoparticles. *Small* **2011**, *8*, 174–202.
24. Haick, H. Chemical Sensors Based on Molecularly Modified Metallic Nanoparticles. *J. Phys. D: Appl. Phys.* **2007**, *40*, 7173–7186.
25. Berry, V.; Saraf, R. F. Modulation of Electron Tunneling in a Nanoparticle Array by Sound Waves: An Avenue to High-Speed, High-Sensitivity Sensors. *Small* **2011**, *7*, 2485–2490.
26. Ko, J. W.; Woo, J. M.; Ahn, J.; Cheon, J. H.; Lim, J. H.; Kim, S. H.; Chun, H.; Kim, E.; Park, Y. J. Multi-Order Dynamic Range DNA Sensor Using a Gold Decorated SWCNT Random Network. *ACS Nano* **2011**, *5*, 4365–4372.
27. Mao, S.; Lu, G.; Yu, K.; Bo, Z.; Chen, J. Specific Protein Detection Using Thermally Reduced Graphene Oxide Sheet Decorated with Gold Nanoparticle-Antibody Conjugates. *Adv. Mater.* **2010**, *22*, 3521–3526.
28. Schwartz, J. J.; Quake, S. R. High Density Single Molecule Surface Patterning with Colloidal Epitaxy. *Appl. Phys. Lett.* **2007**, *91*, 083902-1-3.
29. Shipway, A. N.; Katz, E.; Willner, I. Nanoparticle Arrays on Surfaces for Electronic, Optical, and Sensor Applications. *ChemPhysChem* **2000**, *1*, 18–52.
30. Cheng, J. Y.; Ross, C. A.; Smith, H. I.; Thomas, E. L. Templated Self-Assembly of Block Copolymers: Top-Down Helps Bottom-Up. *Adv. Mater.* **2006**, *18*, 2505–2521.
31. Stoltenberg, R. M.; Liu, C.; Bao, Z. Selective Surface Chemistry Using Alumina Nanoparticles Generated from Block Copolymers. *Langmuir* **2011**, *27*, 445–451.
32. Kim, T. H.; Lee, J.; Hong, S. Highly Selective Environmental Nanosensors Based on Anomalous Response of Carbon Nanotube Conductance to Mercury Ions. *J. Phys. Chem. C* **2009**, *113*, 19393–19396.
33. Liu, J.; Lu, Y. Rational Design of "Turn-On" Allosteric DNAzyme Catalytic Beacons for Aqueous Mercury Ions with Ultrahigh Sensitivity and Selectivity. *Angew. Chem., Int. Ed.* **2007**, *46*, 7587–7590.
34. Cai, S.; Lao, K.; Lau, C.; Lu, J. "Turn-On" Chemiluminescence Sensor for the Highly Selective and Ultrasensitive Detection of Hg^{2+} Ions Based on Interstrand Cooperative Coordination and Catalytic Formation of Gold Nanoparticles. *Anal. Chem.* **2011**, *83*, 9702–9708.
35. Zeng, S. W.; Yong, K. T.; Roy, I.; Dinh, X. Q.; Yu, X.; Luan, F. A Review on Functionalized Gold Nanoparticles for Biosensing Applications. *Plasmonics* **2011**, *6*, 491–506.
36. Wang, Z. X.; Ma, L. N. Gold Nanoparticle Probes. *Coord. Chem. Rev.* **2009**, *253*, 1607–1618.
37. Locklin, J.; Li, D. W.; Mannsfeld, S. C. B.; Borkent, E. J.; Meng, H.; Advincula, R.; Bao, Z. Organic Thin Film Transistors Based on Cyclohexyl-Substituted Organic Semiconductors. *Chem. Mater.* **2005**, *17*, 3366–3374.
38. DeLongchamp, D. M.; Ling, M. M.; Jung, Y.; Fischer, D. A.; Roberts, M. E.; Lin, E. K.; Bao, Z. Thickness Dependence of Microstructure in Semiconducting Films of an Oligofluorene Derivative. *J. Am. Chem. Soc.* **2006**, *128*, 16579–16586.
39. Virkar, A.; Mannsfeld, S.; Oh, J. H.; Toney, M. F.; Tan, Y. H.; Liu, G.; Scott, J. C.; Miller, R.; Bao, Z. The Role of OTS Density on Pentacene and C(60) Nucleation, Thin Film Growth, and Transistor Performance. *Adv. Funct. Mater.* **2009**, *19*, 1962–1970.
40. Wang, Z.; Lee, J. H.; Lu, Y. Highly Sensitive "Turn-On" Fluorescent Sensor for $Hg^{(2+)}$ in Aqueous Solution Based on Structure-Switching DNA. *Chem. Commun.* **2008**, 6005–6007.
41. Miyake, Y.; Togashi, H.; Tashiro, M.; Yamaguchi, H.; Oda, S.; Kudo, M.; Tanaka, Y.; Kondo, Y.; Sawa, R.; Fujimoto, T.; *et al.* Mercury$^{(II)}$-Mediated Formation of Thymine−Hg^{II}−Thymine Base Pairs in DNA Duplexes. *J. Am. Chem. Soc.* **2006**, *128*, 2172–2173.
42. Stoliar, P.; Bystrenova, E.; Quiroga, S. D.; Annibale, P.; Facchini, M.; Spijkman, M.; Setayesh, S.; de Leeuw, D.; Biscarini, F. DNA Adsorption Measured with Ultra-Thin Film Organic Field Effect Transistors. *Biosens. Bioelectron.* **2009**, *24*, 2935–2938.
43. Lee, C. Y.; Gong, P.; Harbers, G. M.; Grainger, D. W.; Castner, D. G.; Gamble, L. J. Surface Coverage and Structure of Mixed DNA/Alkylthiol Monolayers on Gold: Characterization by XPS, NEXAFS, and Fluorescence Intensity Measurements. *Anal. Chem.* **2006**, *78*, 3316–3325.
44. Zhou, X.; Goh, S. H.; Lee, S. Y.; Tan, K. L. X-Ray Photoelectron Spectroscopic Studies of Interactions Between Poly (*p*-vinylphenol) and Poly(vinylpyridine)s. *Appl. Surf. Sci.* **1997**, *119*, 60–66.
45. Li, C. M.; Dong, H.; Cao, X. D.; Luong, J. H. T.; Zhang, X. Implantable Electrochemical Sensors for Biomedical and Clinical Applications: Progress, Problems, and Future Possibilities. *Curr. Med. Chem.* **2007**, *14*, 937–951.
46. Chrisey, L. A.; Lee, G. U.; O'Ferrall, C. E. Covalent Attachment of Synthetic DNA to Self-Assembled Monolayer Films. *Nucleic Acids Res.* **1996**, *24*, 3031–3039.
47. Capua, E.; Natan, A.; Kronik, L.; Naaman, R. The Molecularly Controlled Semiconductor Resistor: How Does it Work?. *ACS Appl. Mater. Interfaces* **2009**, *1*, 2679–2683.
48. Maddalena, F.; Kuiper, M. J.; Poolman, B.; Brouwer, F.; Hummelen, J. C.; de Leeuw, D. M.; De Boer, B.; Blom, P. W. M. Organic Field-Effect Transistor-Based Biosensors Functionalized with Protein Receptors. *J. Appl. Phys.* **2010**, *108*, 124501−1−4.
49. Park, Y. M.; Salleo, A. Dual-Gate Organic Thin Film Transistors as Chemical Sensors. *Appl. Phys. Lett.* **2009**, *95*, 133307−1−3.
50. Nolan, E. M.; Lippard, S. J. Tools and Tactics for the Optical Detection of Mercuric Ion. *Chem. Rev.* **2008**, *108*, 3443–3480.
51. Bings, N. H.; Bogaerts, A.; Broekaert, J. A. C. Atomic Spectroscopy. *Anal. Chem.* **2006**, *78*, 3917–3945.
52. McNicholas, T. P.; Zhao, K.; Yang, C.; Hernandez, S. C.; Mulchandani, A.; Myung, N. V.; Deshusses, M. A. Sensitive Detection of Elemental Mercury Vapor by Gold-Nanoparticle-Decorated Carbon Nanotube Sensors. *J. Phys. Chem. C* **2011**, *115*, 13927–13931.
53. Ojea-Jiménez, I.; López, X.; Arbiol, J.; Puntes, V. Citrate-Coated Gold Nanoparticles as Smart Scavengers for Mercury(II) Removal from Polluted Waters. *ACS Nano*, **2012**, In Press, DOI:10.1021/nn204313a.
54. Kantouch, A.; El-Sayed, A. A. Polyvinyl Pyridine Metal Complex as Permanent Antimicrobial Finishing for Viscose Fabric. *Int. J. Biol. Macromol.* **2008**, *43*, 451–455.
55. Manceau, M.; Rivaton, A.; Gardette, J.-L.; Guillerez, S.; Lemaitre, N. The Mechanism of Photo- and Thermooxidation of Poly(3-hexylthiophene) (P3HT) Reconsidered. *Polym. Degrad. Stab.* **2009**, *94*, 898–907.
56. Arnold, M.; Cavalcanti-Adam, E. A.; Glass, R.; Blümmel, J.; Eck, W.; Kantlehner, M.; Kessler, H.; Spatz, J. P. Activation of Integrin Function by Nanopatterned Adhesive Interfaces. *ChemPhysChem* **2004**, *5*, 383–388.
57. Meng, H.; Zheng, J.; Lovinger, A. J.; Wang, B. C.; Van Patten, P. G.; Bao, Z. Oligofluorene-Thiophene Derivatives as High-Performance Semiconductors for Organic Thin Film Transistors. *Chem. Mater.* **2003**, *15*, 1778–1787.
58. Sokolov, A. N.; Cao, Y.; Johnson, O. B.; Bao, Z. Mechanistic Considerations of Bending-Strain Effects within Organic Semiconductors on Polymer Dielectrics. *Adv. Funct. Mater.* **2011**, *22*, 175–183.
59. Roberts, M. E.; Mannsfeld, S. C. B.; Stoltenberg, R. M.; Bao, Z. Flexible, Plastic Transistor-Based Chemical Sensors. *Org. Electron.* **2009**, *10*, 377–383.